We are IntechOpen,
the world's leading publisher of
Open Access books
Built by scientists, for scientists

6,900
Open access books available

186,000
International authors and editors

200M
Downloads

Our authors are among the

154
Countries delivered to

TOP 1%
most cited scientists

12.2%
Contributors from top 500 universities

CLARIVATE ANALYTICS

BOOK CITATION INDEX

INDEXED

WEB OF SCIENCE™

Selection of our books indexed in the Book Citation Index
in Web of Science™ Core Collection (BKCI)

Interested in publishing with us?
Contact book.department@intechopen.com

Laser Beam Welding of Austenitic Stainless Steels – Similar Butt and Dissimilar Lap Joints

Abdel-Monem El-Batahgy

Additional information is available at the end of the chapter

1. Introduction

1.1. Laser beam welding of similar butt joints of austenitic stainless steels

Because of its inherent corrosion resistance, austenitic stainless steels, known as 300 series, have become cost-effective, staple materials for long-term applications in many industrial sectors including gas, petroleum, petrochemicals, fertilizers, food processing, and pulp industries as well as power generating plants. They have found also widespread use for manufacturing of chemical installations including stationary pressure tanks and tanks for transport of liquid and compressed gases, pipelines of high diameter in water power plants, for manufacturing of ships for transport of chemicals and installations of drilling rigs, etc. Thick-section stainless steels are widely used in the components and structures for nuclear power plants.

For all applications of austenitic stainless steels, welding is of considerable importance since it is widely used in components' manufacturing. In comparison with ferritic steels, lower thermal conductivity and higher thermal expansion coefficient of austenitic stainless steels results in larger thermal distortions and internal stresses of the welded parts, which increase susceptibility of the weld to hot cracks.

Another possible welding problem of austenitic stainless steels is sensitization that occurs at 900-1400ºF (482-760ºC) during cooling after welding where chromium carbides form along the austenite grains and causes depletion of chromium from the grains resulting in decreasing the corrosion protective passive film.

In this concern, austenitic stainless steels poses distinct challenges when it is joined with gas tungsten arc welding (GTAW) due higher possibility of carbide precipitation and distortion in comparison with laser welding. In other words, joining austenitic stainless steels with

GTAW can be tricky, but with a laser, it can be done successfully. Previous studies of the weldability of stainless steels indicate that the basic condition for ensuring high quality of welded joints and reducing thermal distortions to minimum is reducing the heat input of welding that is ensured only by laser welding.

CO_2 laser beam welding with a continuous wave, which is widely used for stainless steels components, is a high energy density and low heat input process. The result of this is a small heat-affected zone (HAZ), which cools very rapidly with very little distortion, and a high depth-to-width ratio for the fusion zone.

The heat flow and the fluid flow in the weld pool can significantly influence the temperature gradients, the cooling rates and the solidification structure. In addition, the fluid flow and the convective heat transfer in the weld pool are known to control the penetration and shape of the fusion zone [1].

Generally, laser beam welding involves many variables; laser power, welding speed, defocusing distance and type of shielding gas, any of which may have an important effect on heat flow and fluid flow in the weld pool. This in turn will affect penetration depth, shape and final solidification structure of the fusion zone. Both the shape and microstructure of the fusion zone will considerably influence the properties of the weldment.

There are many reports [2-4] that deal with the shape and solidification structure of the fusion zone of laser beam welds in relation to different laser parameters. However, the effect of all influencing factors of laser welding has up to now not been extensively researched. More work is required for understanding the combined effect of laser parameters on the shape and microstructure of the fusion zone.

The present investigation is concerned with laser power, welding speed, defocusing distance and type of shielding gas and their effects on the fusion zone shape and final solidification structure of some austenitic stainless steels.

1.2. Experimental procedure

Three types of commercial austenitic stainless steels, 304L, 316L and 347, were used. Their chemical composition and mechanical properties are given in Table 1. The thickness of both 304L and 316L steels was 3 mm while that of 347 steel was 5 mm.

Base metal	Cr	Ni	Mn	C	Si	P	S	Mo	Cb	TS (MPa)	YS (MPa)	Elong. (%)
304L	18.2	8.5	1.7	0.025	0.35	0.03	0.01	0.20	0.01	235	309	32
316L	16.5	10.5	1.9	0.02	0.38	0.02	0.01	2.27	0.01	556	317	31
347	17.7	9.7	1.8	0.04	0.40	0.03	0.01	0.25	0.35	577	345	39

Table 1. Chemical composition (wt%) and mechanical properties of the used base metals

Both bead-on-plate and autogenous butt weld joints were made using a carbon dioxide laser capable of producing a maximum output of 5 kW in the continuous wave mode. Bead-on plate was made on plates with 3 mm thickness while autogenous butt weld joints were made on plates with 3 and 5 mm thickness. Specimens with machined surfaces were prepared as square butt joints with dimensions of 125x150 mm and were held firmly using fixture to prevent distortion

The laser beam welding parameters investigated are summarized in Table 2. Combinations of laser power (P) of 2-5 kW and speed (S) of 0.5-3 m/min resulted in nominal heat in nominal heat inputs (HI) ranging from 0.04 to 0.48 kJ/mm. The defocusing distance (D_d) was in the range of -5 to 3 mm. Shielding was made using either argon or helium gas.

Weld joint/ Thickness (mm)	P (kW)	S (m/min)	HI (kJ/mm)	D_d (mm)	Shielding gas/ Flow rate(1/min)
BOP / 3	2	3	0.04	0.0, -1.0, -2.0,-3.0, -4.0,-5.0, +1.0,+2.0, +3.0	argon / 15
Butt / 3	3	0.5, 1, 2, 3	0.36, 0.18, 0.09, 0.06	0.0	argon / 15
Butt / 3	4	0.5, 1, 2, 3	0.48, 0.24, 0.12, 0.08	0.0	argon / 15
Butt / 3	4	3	0.08	0.0, -0.2, -0.4, -0.6	argon/15
Butt / 3	4	3	0.08	0.0, -0.2	helium / 15
Butt / 5	5	1, 2, 3	0.3, 0.15, 0.1	0.0. -0.2, -0.4	argon/15

Table 2. Welding parameters used

After welding, the specimens were visually inspected then, sectioned transverse to the welding direction. The shape and microstructure of the fusion zone were examined using optical microscopy. Micro-compositional analysis of welds was performed using an electron probe micro-analyzer (EPMA) at an accelerating voltage of 25 kV.

Mechanical tests including tensile, bending and hardness measurements of butt welds having complete penetration were performed according to relevant standards. The data reported are the average of three individual results.

1.3. Results and discussion

1.3.1. Macrostructure of laser beam welds

1.3.1.1. Effect of laser power

The effect of heat input as a function of laser power, HI = P/S, was clarified using type 304L and type 316L steels. Both welding speed and defocusing distance were kept constant at 3 m/min and zero respectively.

The penetration depth increased sharply with increasing laser power from 2 to 3 kW as shown in Figure 1. Complete penetration for the 3mm base metal was obtained at laser power equal to or greater than 4 kW. Figure 9 shows an example of a cross section of type 304L steel butt weld made using laser power of 4 kW. The weld bead showed a characteristic of laser welding with dept / width ratio close to 3. No welding cracks or porosity were found in any of the welds, this may be partly due to the good crack resistance of the base metal and the welding conditions provided.

The results indicated also that the development of the weld pool is essentially symmetrical about the axis of the laser beam. Yet, lack of symmetry at the root side was observed particularly at higher welding speed (Figure 2) suggesting an unsteady fluid flow in the weld pool. This is due to the presence of two strong and opposing forces, namely, the electromagnetic and the surface tension gradient forces. At these locations, the electromagnetic force may have overcome the surface tension force, thereby, influencing convective heat transfer. As a result, any local perturbation in the weld pool can cause the flow field to change dramatically, resulting in the observed lack of local symmetry.
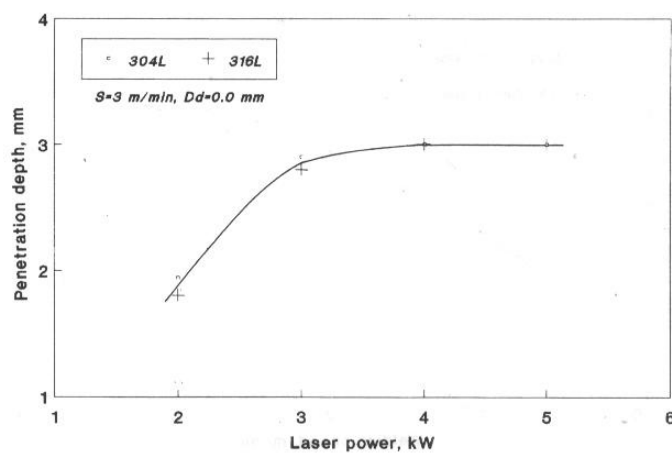

Figure 1. Effect of laser power on penetration depth of types 304L and 316L stainless steel welds.
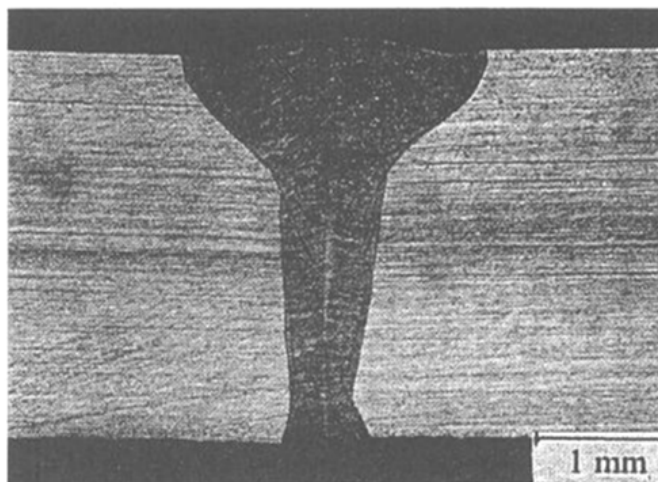

Figure 2. A cross section of type 304L stainless steel weld made using P=4kW, S=3m/min, D$_d$=0.0mm.

Laser power has a less influence on both weld profile and HAZ width in comparison with its effect on penetration depth. This is in agreement with other researchers work where they pointed out that changing laser power between 3 and 5 kW [5] did not result in any significant change in the size or shape of the weld.

It is expected that similar results concerning the dependence of penetration depth on laser power could be obtained in the case of type 347 steel due to similarity in both physical and mechanical properties. The optimum power for complete penetration with acceptable weld profile for the 5mm base metal thickness was 5 kW at a welding speed of 2 m/min as shown in Figure 3.
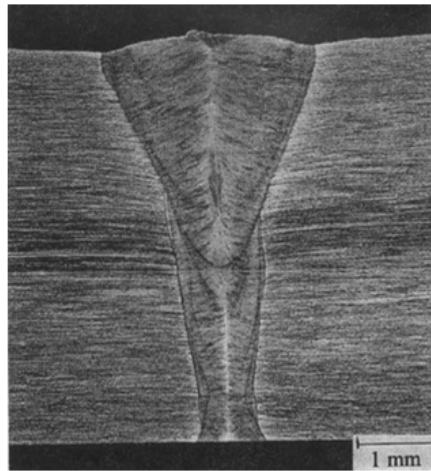

Figure 3. Optimum weld profile of type 347 stainless steel made using P=5kW, S=2m/min, D_d=-0.4mm.

1.3.1.2. Effect of welding speed

The effect of welding speed was investigated at the optimum laser power (4 kW) and zero defocusing distance. Figure 4 shows the relationship between welding speed and fusion zone depth/width ratio for both 304L and 316L base metals. The depth/width ratio increased sharply from 2.1 to 4.1 with the increase in welding speed from 0.5 to 3 m/min.

The dependence of depth/width ratio on welding speed was confirmed at a different laser power (3 kW). A lower welding speed resulted in a considerable increase in the fusion zone size and consequently a decrease in depth/width ratio leading to unacceptable weld profile. Complete penetration with relatively acceptable fusion zone size for the 3mm base metal thickness was obtained at welding speed of 2 m/min as shown in Figure 5. The fusion zone is symmetrical about the axis of the laser beam.

The above results have shown that the laser power and welding speed should be optimized in order to minimize heat input, then a satisfactory weld with reliable quality could be obtained. This reflects one of the most notable features of laser welding compared with other welding processes, which is small heat input.

Turning to the macrographs shown in Figures 5 and 8, complete penetration with relatively acceptable fusion zone profile could be obtained using either 4 kW, 3 m/min (Figure 5) or 3

kW, 2 m/min (Figure 8). However, 4 kW, 3 m/min resulted in a smaller fusion zone size with less inflection at its interface in addition to the high welding speed in this case.
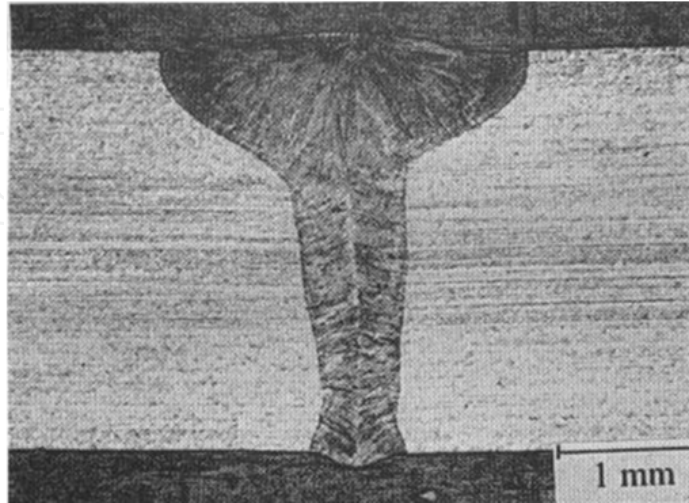

Figure 4. Influence of welding speed on weld depth/width ratio of types 304L and 316L stainless steels.
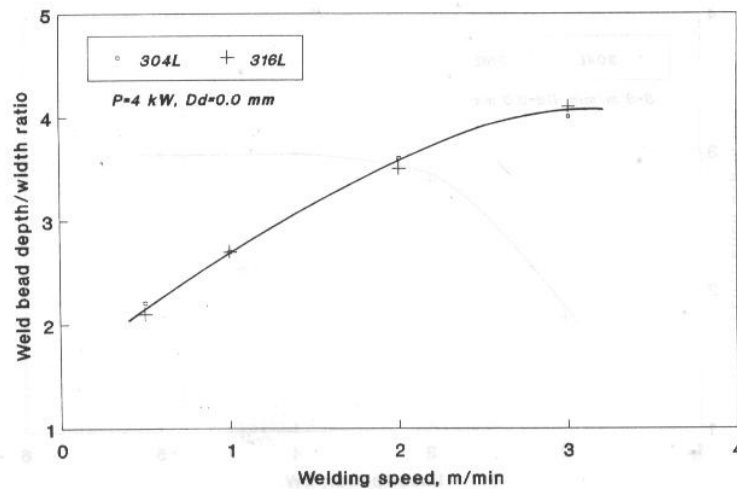

Figure 5. A cross section of type 304L stainless steel weld made using P=3kW, S=2m/min, D_d=0.0mm.

At high welding speed, attenuation of beam energy by plasma is less significant. This results in relatively more exposure of the laser beam on the sample surface. Consequently, the depth/width ratio would be increased and the fusion zone size would be minimized.

1.3.1.3. Effect of defocusing distance

Defocusing distance, focus position, is the distance between specimen surface and the optical focal point. In order to study its effect on both penetration depth and weld profile, bead-on-plate was made with changing defocusing distance between -5 and 3 mm. Low laser power (2 kW) and high welding speed (3 m/min) were selected to obtain incomplete penetration.

Examples of weld cross sections of type 304L steel made using different defocusing distances are shown in Figure 6. No cracking or porosity was observed in all welds. The penetration depth is considerably decreased with changing defocusing distance from zero (Figure 6-b) to either minus (Figure 6-a) or plus (Figure 6-c) values as a result of decreasing laser beam density.

The relationship between defocusing distance and penetration depth of both 304L and 316L steels is summarized in Figure 7. The penetration depth decreased from 1.9 to 1.6 mm on changing the defocusing distance from zero to either -1 or 1mm. Then, the penetration depth decreased sharply to about 0.2 mm on changing the defocusing distance to more negative (-5 mm) or positive (4 mm) values.

These results indicated that the most effective range of defocusing distance to get maximum penetration with acceptable weld profile lies between zero and -1 mm. In order to obtain the optimum value, complete penetration butt welds were made using previously obtained optimum laser power (4 kW) and optimum welding speed (3 m/min). The most acceptable weld profile was obtained at defocusing distance of - 0.2 mm for 3 mm thickness where weld bead depth/width ratio is maximum and fusion zone size is minimum with a slight taper configuration as shown in Figure 8. However, the optimum defocusing distance to attain acceptable weld profile for 5 mm thickness was -0.4 mm (Figure 3). The smooth curved and symmetrical fusion zone interface shown in Figures 3 and 8 suggests that the driving forces for fluid flow in the weld pool, buoyancy and surface tension gradient, augment each other, resulting in a coherent flow field.
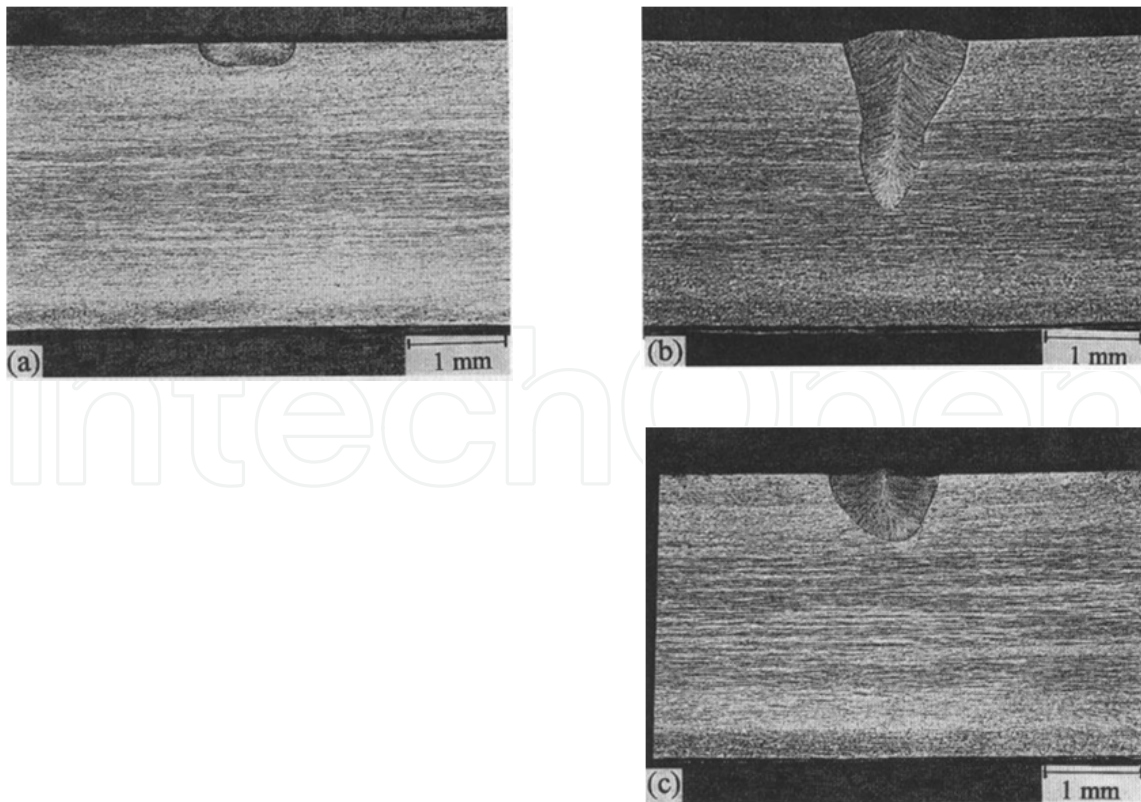

Figure 6. Cross section of type 304L stainless steel welds made using P=2kW, S=3m/min with different defocusing distances. (a) D_d=-3.0mm, (b) D_d=0.0mm, (c) D_d=+2.0mm.
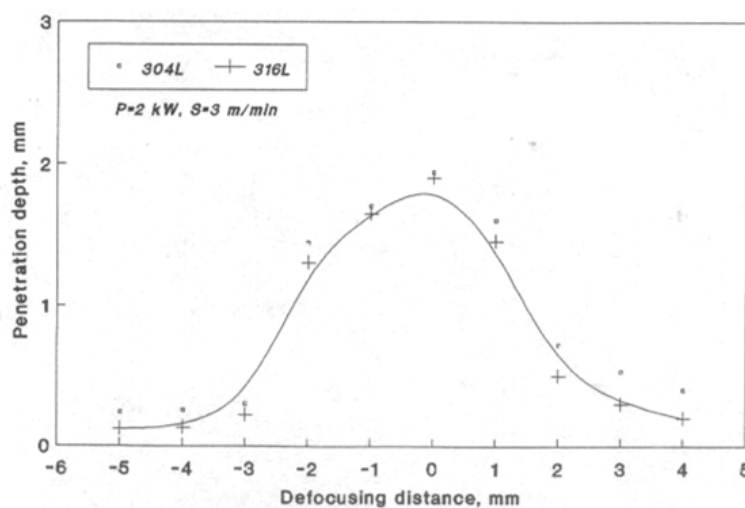
Figure 7. Relationship between defocusing distance and penetration depth of types 304L and 316L stainless steels.
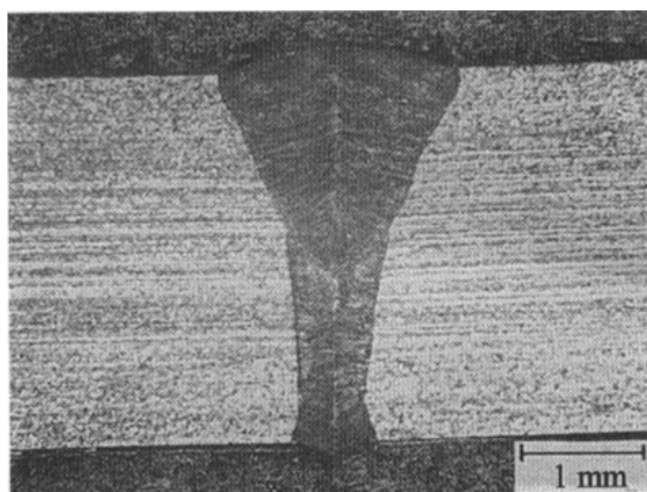

Figure 8. A cross section of type 304L stainless steel weld made using P=4kW, S=3m/min, D$_d$=-0.2mm.

1.3.1.4. Effect of type of shielding gas

In all previous experiments, argon was used as a shielding gas. For comparison, argon was replaced by helium while other laser parameters were kept constant. Weld profile is remarkably improved where fusion zone interfaces are almost parallel to each other as shown in Figure 9.

In general, when the laser beam interacts with the workpiece, a hole is drilled through the thickness of the material. This hole or cavity is filled with a plasma and surrounded by molten metal, thus, the high energy density of the focused beam could be lost easily. This plasma effect was reduced as a result of the higher ionization potential of helium then, the weld profile was improved.
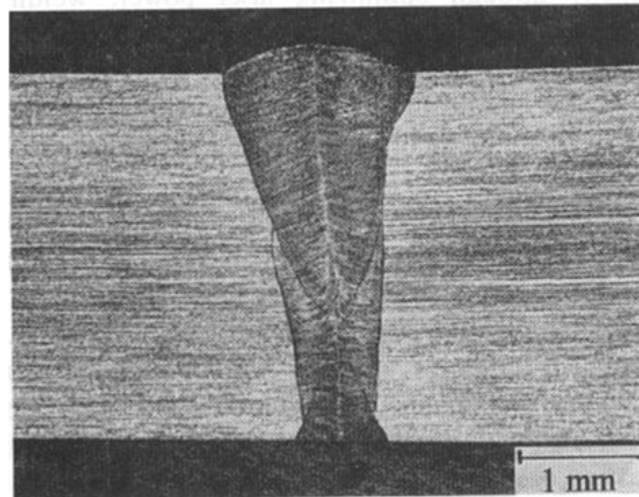
Figure 9. Optimum weld profile of type 304L stainless steel obtained using helium as a shielding gas instead of argon with the same laser parameters as of Figure 15.

1.3.2. Microstructure of laser beam welds

Microstructures of type 304L steel weld metals made using two different welding speeds, 1 and 3 m/min, with same laser power, 4 kW, are shown in Figure 10. The noticeable feature is the highly directional nature of the microstructure around the axis of the laser beam. This is due to solidification of the weld metal at high cooling rate compared to that of conventional GTA welding [6]. It can also be noticed that the higher the welding speed, the finer the dendritic structure (Figure 10-b). This is attributed to an increase in both solidification and cooling rates due to low heat input resulted from high welding speed.
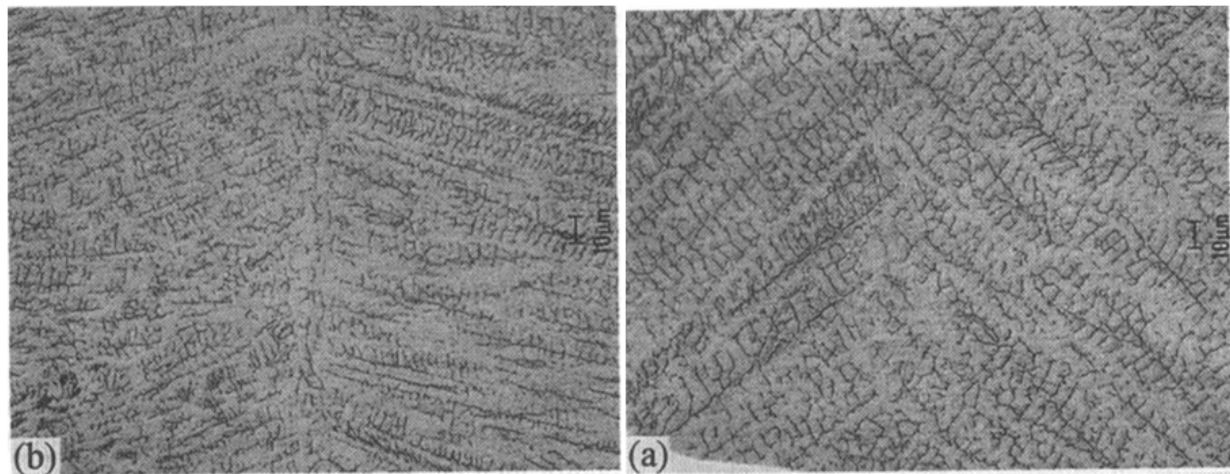

Figure 10. Optical micrographs of weld metals of type 304L stainless steel made using P=4kW with different welding speeds. (a) S=1m/min, (b) S=3m/min.

Concerning the effect of laser power, the higher the laser power, the coarser is the dendritic structure due to decreasing cooling rate. However, the effect of laser power was relatively less than that of welding speed.

The microstructures of all laser beam welds were always austenite with a few percent of delta-ferrite at the dendritic boundaries. The existence of delta-ferrite was confirmed by both colour etching and electron probe microanalysis (EPMA). The amount of delta-ferrite was estimated using Cr and Ni equivalents [7] of weld metal chemical composition. Based on the Schaeffler diagram, about 2 or 3 vol% ferrite was expected to exist in the austenitic matrix. It should be reported that no weld solidification cracking was observed in any of the welds evaluated.

Under normal weld solidification conditions, the solidification mode in austenitic stainless steels is primarily a function of composition, with a shift from primary ferrite to primary austenite accomplished by reducing the Cr_{eq}/Ni_{eq} ratio below 1.5 [8].

However, Suutala [2], Vitek and David [9], and Lippold [10] have illustrated that the boundary between primary austenite and primary ferrite solidification is not just a function of weld metal composition, but is a function of the growth rate.

The subject results are consistent with the modified Suutala diagram [11] for predicting microstructure and cracking of austenitic stainless steels under rapid weld solidification conditions encountered during laser welding. All the steels tested exhibited a Cr_{eq}/Ni_{eq} ratio greater than 1.7, the value suggested by the modified Suutala diagram as the demarcation of crack susceptibility. Consequently, it can be deduced that all welds concerned in this investigation were solidified as mixed mode of primary and massive austenite. The transition in primary solidification from ferrite to austenite could be attributed to weld pool undercooling as a result of extremely high solidification growth rate [12-15].

The results are also in agreement with Lippold [12] work where he pointed out that cracking in austenitic stainless steel welds is avoided as the proportion of primary ferrite in the mixed mode solidification increases.
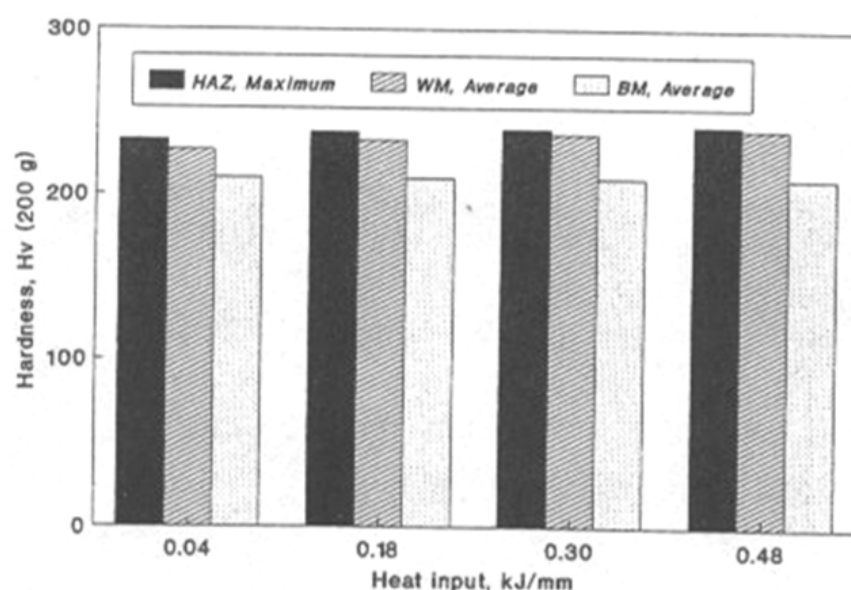

Figure 11. Hardness profiles of base metal, HAZ and weld metal of type 304L stainless steel as a function of heat input.

1.3.3. Mechanical properties

Tensile test results of all laser butt welds with complete penetration showed that failure has taken place in the base metal. The bending test at room temperature showed no cracks in all joints as a result of high ductility.

Typical hardness profiles of the base metal, HAZ and weld metal of type 304L steel as a function of heat input are shown in Figure 11. No significant difference between hardness of the base metal and that of weld metal or HAZ was obtained. Hardness of both weld metal and HAZ was slightly higher than that of the base metal regardless of heat input. These results were also valid for the other two base metals. This is expected because mechanical properties of steel, in general, are based on its microstructure.

2. Laser beam welding of austenitic stainless steel in lap joints with zn-coated carbon steel

2.1. Introduction

Because of its excellent corrosion resistance, austenitic stainless steel has found widespread use in the paper making equipment includes pressure vessels, storage tanks, piping, hopper, bins, chutes and structural components. For all of these applications, attachments such as access platforms, catwalks, stiffeners, column supports, stairways, washers and pipe hangers are welded to the outside surfaces of the equipment. Zn-coated carbon steel is often specified for these attachments due to its good corrosion resistance and lower cost. Lap weld joints of Zn-coated steel to austenitic stainless steel are used also in other fields such as plate-tube joints, radiators, washing machines as well as some components in the aeronautic field [16].

Although welding of Zn-coated steel to austenitic stainless steel is a common practice, it presents serious problems concerning with weld zone porosity and LME cracking of austenitic stainless steel base metal due to zinc vaporization. These welding problems have been studied in the case of conventional metal arc welding processes [17]. It is reported that joining gaps between the sheets to be lap welded are adjusted in order to enable the degasification of zinc vapour.

On the other hand, laser butt and lap weld joints of both similar and dissimilar materials are being used in many industrial applications. The fraction of laser welding in all industrial applications is about 15-25% which varies from country to country [18-20]. The most notable features of laser welding compared with other conventional welding processes are the high weld quality and high welding speed. This together with its low heat input makes laser a most hopeful candidate for thin sheet metal welding.

However, similar problems as in conventional metal-arc-welding of Zn-coated steel to austenitic stainless steel are expected also in case of laser beam welding. Therefore, more work is required for understanding these problems and the factors affecting them.

This investigation has been concerned with CO_2 laser welding of austenitic stainless steel in lap joints with Zn-coated carbon steel. The focus was made on weld joint quality in terms of weld profile, porosity in the weld zone and liquid metal emrittlement (LME) cracking of the austenitic stainless steel base metal. The influence of type and flow rate of shielding gas, gap between the sheets and zinc removal prior to welding was clarified. Quality of weld joints was evaluated as a function of weld zone shape, porosity and LME cracking of austenitic stainless steel base metal.

2.2. Experimental procedure

Commercial types of ASTM A36, 0.7 mm thick carbon steel sheet coated with 10 μm zinc on both sides and ASTM A240 Type 304L, 1mm thick stainless steel sheet were used for dissimilar lap joints. Table 3 shows their chemical composition and mechanical properties.

Base Metal	C	Mn	Si	S	P	Cr	Ni	YS (N/mm²)	UTS (N/mm²)	Elong (%)
Zn-coated	0.04	0.35	0.26	0.01	0.02	-	-	245	377	27
304L	0.04	1.70	0.35	0.01	0.03	18.2	8.5	359	558	32

Table 3. Chemical composition (wt%) and mechanical properties of used base metals

Pairs of these dissimilar steel sheets of 150x150 mm were welded with an overlap of 50 mm and with weld bead at the middle of the overlap. Zn-coated steel sheet was upper-most and the joint was clamped 15 mm on both sides of the weld line along its entire length. Configurations of laser lap weld specimen are shown in Figure 12. All specimens were ultrasonically cleaned to remove dirt and oil prior to welding.
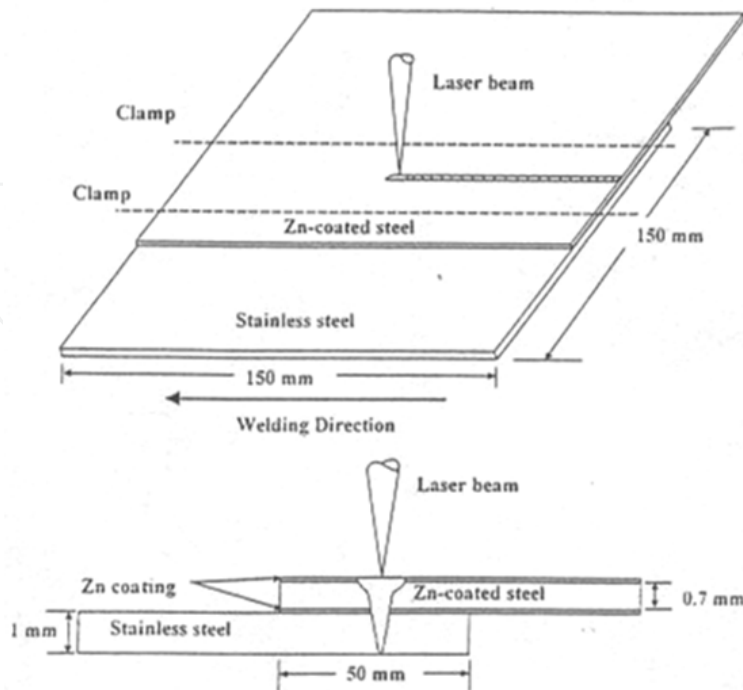

Figure 12. Configuration of the used laser lap weld specimen.

Welding was performed using CO_2 laser with a maximum output of 3 kW operated in multi-mode. The beam was focused using a parabolic mirror with 150 mm focal length. Laser beam welding parameters used are summarized in Table 4. Optimizing laser power, welding speed and focal point position is of considerable importance for the weld quality in terms of fusion zone size and profile. In order to clarify the influence of shielding gas, gap between the sheets and pre-weld zinc removal on weld quality, laser power, welding speed, and defocusing distance (focal point position) were optimized and kept constant at 2.5 kW, 3 m/min, and 0.1 mm below specimen surface respectively. Shielding was done using argon or helium with flow rate of 15~30 l/min. Prescribed gap ranging from 0.025 to 0.3 mm was introduced between the sheets along the clamped areas of the welding fixture. Pre-weld zinc removal from the weld area was done by grinding.

P (KW)	S (m/min)	Dd (mm)	Shielding gas Type Flow rate (1/min)	Gap between Sheets (mm)	Zinc removal prior to Welding
2.5	3	-0.1	Argon 15 ~ 30	No	No
2.5	3	-0.1	Helium 15 ~ 30	No	No
2.5	3	-0.1	Argon 15	0.025 ~ 0.3	No
2.5	3	-0.1	Helium 15	0.025 ~ 0.3	No
2.5	3	-0.1	Argon 15	No	Yes
2.5	3	-0.1	Helium 15	No	Yes

Table 4. Laser welding parameters
P: Laser power, S: Welding speed, Dd: Defocusing distance
Working distance: 10 mm at Dd = 0.0 mm, Nozzle diameter: 4mm

After welding, the specimens were subjected to non-destructive testing including visual and dye penetrant test methods then, sectioned transverse to the welding direction. Three sections of each seam weld were prepared for metallographic examinations using standard technique. Quality of the dissimilar lap joints was evaluated as a function of weld profile, porosity level in fusion zone, LME cracking in austenitic stainless steel base metal. Tensile shear test was carried out for all laser lap welded joints and the data reported are the average of three individual results.

2.3. Results and discussion

2.3.1. Effect of shielding gas

Examples of macrographs laser welds produced using argon and helium as a shielding gas with a flow rate of 15 l/min are shown in Figure 13-a and b respectively. It is clear that non-uniform weld beads with large pores were obtained in both cases. However, wide seam width combined with an increase of the frequency of pores was obtained with argon (Figure 13-a). In other words, the number of pores was much less with using helium as a shielding

gas (Figure 13-b). This means that shielding gas type is an essential factor to improve weld quality since it is used to protect the molten metal against oxidation and blow the plasma away from the beam path.

Generally, when welding zinc coated steel with stainless steel there is a very strong plasma formation due to the low boiling point of zinc (906 ^{o}C) and it's high vapour pressure, which is about eight orders of magnitude greater than that of Fe [21]. The high vapourization of zinc increases the pressure of the vapour, which is transformed to plasma in the laser beam, to expand further into the free space above the metal surface. This will affect the absorption and fluctuation of the plasma and in practice this is shown as increased splattering and porosity in the weld. This plasma effect was reduced as a result of the higher ionization potential of helium then, weld quality was improved.

With this relatively low flow rate, the process seemed to change swiftly between deep penetration welds and vapour assisted welds. This may be explained by the presence of zinc, which makes the process unstable due to plasma fluctuation as has reported in prior investigation [22]. Consequently, optimized shielding gas flow rate makes the difference between a good or poor weld.
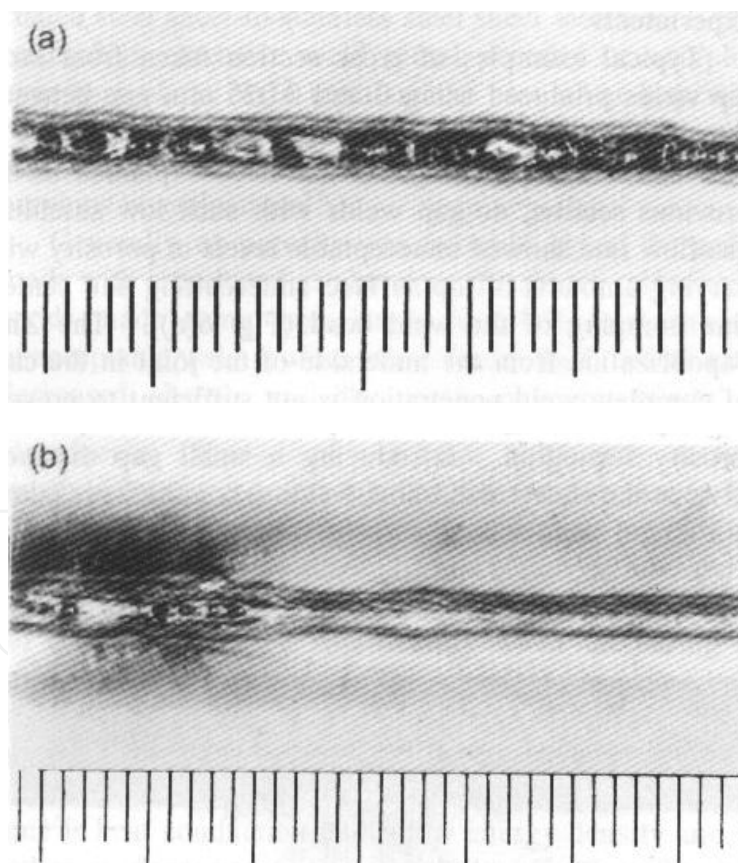

Figure 13. Macrographs of laser welds produced using (a) argon and (b) helium as a shielding gas with 15 l/min flow rate.

With increasing shielding gas flow rate above 15 l/min, the number of pores in seem welds was decreased and weld pool penetration was increased. Examples of macrographs of laser

welds produced using higher flow rate; 30 l/min of argon and helium as a shielding gas are shown in Figure 14. It is obvious that smooth and homogeneous seam welds free from pores were obtained in both cases. The increase in penetration depth obtained in this case is consistent with the expected effect of increased plasma suppression with increased flow rate, i.e. more of the beam was allowed to reach the work-piece. However, there appeared to be a trade-off between plasma suppression effects and weld pool stability with increase shielding gas flow rate.

Turning to shielding gas type, it remarkably affected weld zone profile. Low magnification stereoscopic photographs of cross sections taken from laser welds of Figure 14-a and b are shown in Figure 15-a and b respectively. The use of helium has resulted in complete penetration with higher depth/width ratio and a slight taper configuration which means minimum fusion zone size (Figure 15-b) in comparison with that obtained using argon (Figure 15-a). In other words, helium has a more favorable effect on the molten metal than argon at optimized flow rates, which make the welds more homogeneous and free from pores. A flow rate of 22 l/min for helium was found to be satisfactory in comparison with 30 l/min for argon. These results do conform with prior results of other investigators where they have shown that the weld defects, due to the vapourization of zinc, can be reduced by optimizing shielding gas parameters [23-25].
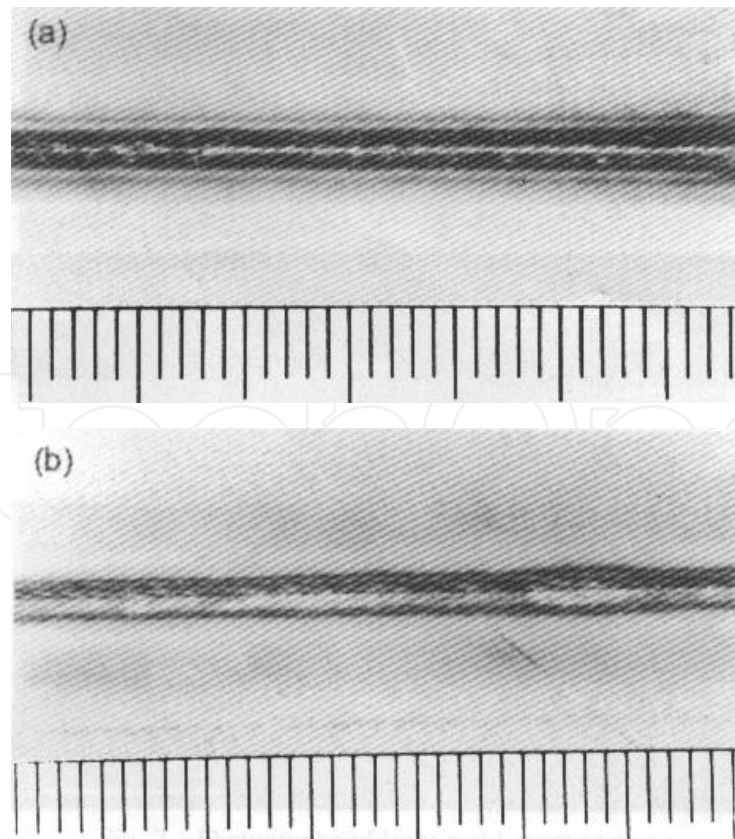

Figure 14. Macrographs of laser welds made using (a) argon and (b) helium as a shielding gas with 30 l/min flow rate.
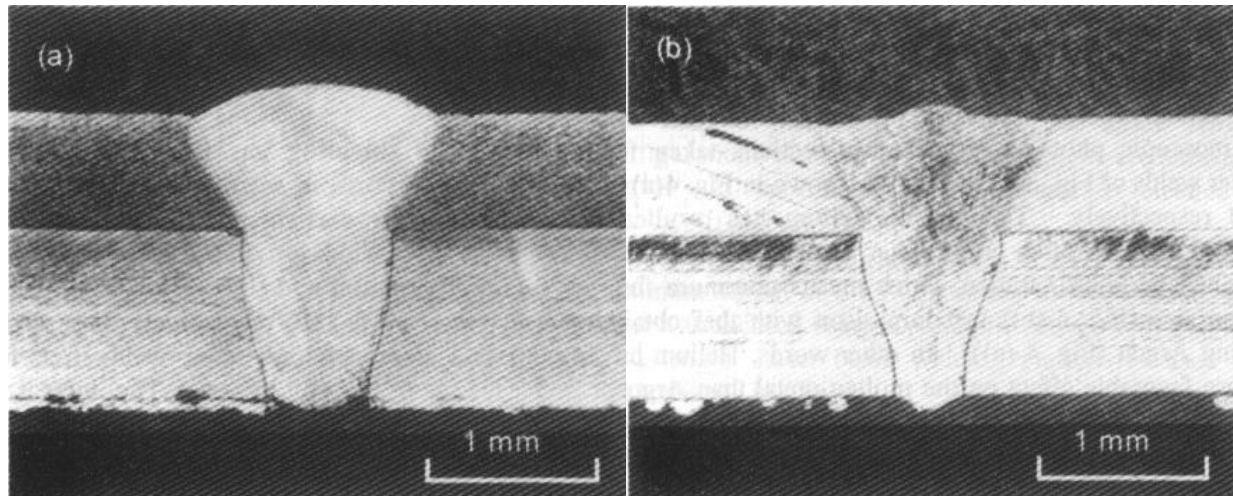
Figure 15. Low magnification stereoscopic photographs of cross sections taken from laser welds of Figure 14

On the other hand, it is found that both type and flow rate of shielding gas have no effect on LME cracking of austenitic stainless steel. Figure 16 shows a typical example of optical micrograph of a cross section taken from lap weld produced using helium with its optimum flow rate; 30 l/min. In spite of obtaining homogeneous, sound, complete penetration and acceptable weld profile with such high flow rate, the noticeable feature is the formation of severe cracking at the stainless steel base metal. These cracking were extended for a distance of about 0.7 mm around both sides of lap weld joints and propagated on grain boundaries. This type of cracking is typical LME cracking of the austenitic stainless steel which occurs above 750°C when it is exposed to molten zinc and tensile stresses. Molten zinc can be produced by the heat of welding and tensile stresses can be generated from the heating and cooling cycles during welding. This cracking type is characterized by extremely rapid crack propagation perpendicular to the applied stress [26]. It should be mentioned also that similar results were obtained for lap weld joints produced using argon gas shielding.
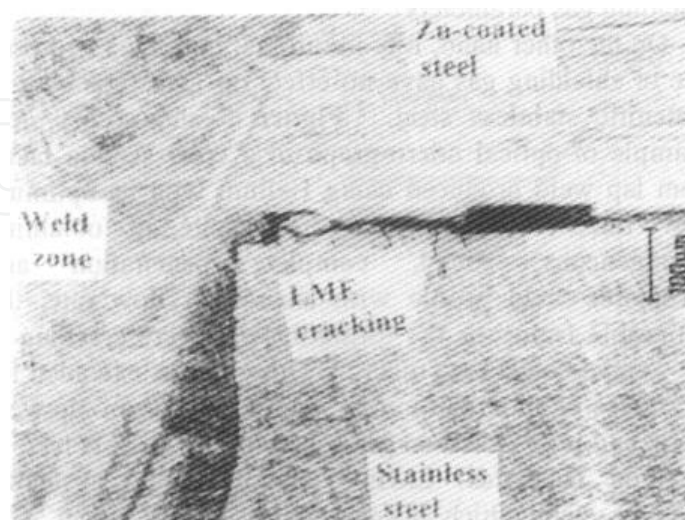

Figure 16. Typical example of optical micrograph of a cross section taken from laser lap weld produced using helium as a shielding gas with its optimum flow rate; 30 l/min.

2.3.2. Effect of gap between the sheets

In the above section, lap welds were made with a good contact, i.e. without a gap between the sheets. In order to clarify its effect on weld joint quality, prescript gap was introduced between the sheets and shielding was done using either argon or helium with its lower flow rate (15 1/min) which resulted in weld porosity in the previous experiments.

Typical examples of cross sections taken from laser lap welds produced using 0.0 and 0.025 mm gap between the sheets in case of helium shielding are shown in Figure 17-a and b respectively. As has been explained in the previous section, no-gap welds with such low shielding gas flow rate showed unacceptable levels of porosity with varying amounts of top surface undercutting and center-line humping of the weld bead (Figure 17-a). The zinc vapourization from the underside of the joint in the case of complete weld penetration is not sufficient to prevent porosity formation. Introducing a small gap distance between the sheets with same welding conditions resulted in a sound weld where porosity was not observed (Figure 17-b). Also, weld profile was remarkably improved where a smooth curved and symmetrical fusion zone interface was obtained.

In other words, acceptable quality for laser lap welds concerning soundness and profile could not be obtained with low shielding gas flow rate and without a gap between the sheets. Once the heat input was sufficient to permit melting through the top sheet, there was explosive ejection of molten weld metal due to vapourization of the zinc layers at the Zn-coated steel sheet-to-stainless steel sheet interface. This resulted in extensive weld metal porosity or complete expulsion of the weld metal in the case of no-gap weld leading to undercutting the top steel sheet, as shown in Figure 17-a. This is in a good agreement with results of previous investigations [27, 28].
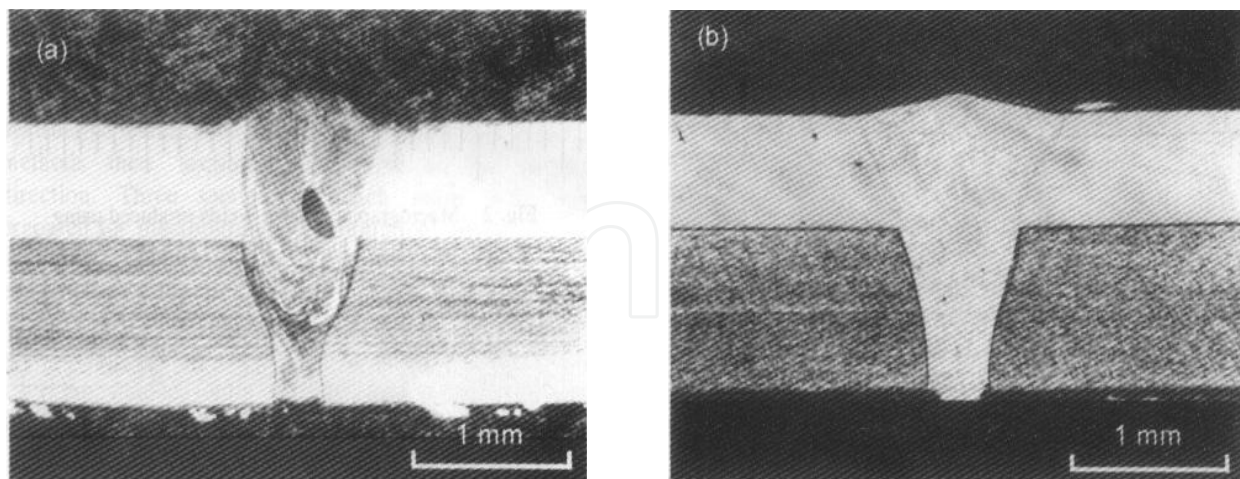

Figure 17. Typical examples of cross sections taken from laser lap welds produced using 15 l/min helium and different gap distances. (a) Gap: 0.0mm, (b) Gap: 0.025mm.

Generally, no porosity was found in any of the welds made with introducing gap between the sheets. However, welds made by gap larger than 0.05 mm showed unacceptable weld profile where weld depth /width ratio decreases sharply and the weld geometry begins to

deteriorate. Photographs of laser weld cross sections produced using 0.1 and 0.3 mm gaps are shown in Figure 18-a and b respectively. A gap distance of 0.1 mm gave a concave top surface, with a relatively low depth/ width ratio (Figure 18-a). The tendency of the molten pool to collapse increased significantly with increasing the gap to higher value. This resulted in remarkable undercut in the welds and excessive drop-through of the weld metal into the gap (Figure 18-b).
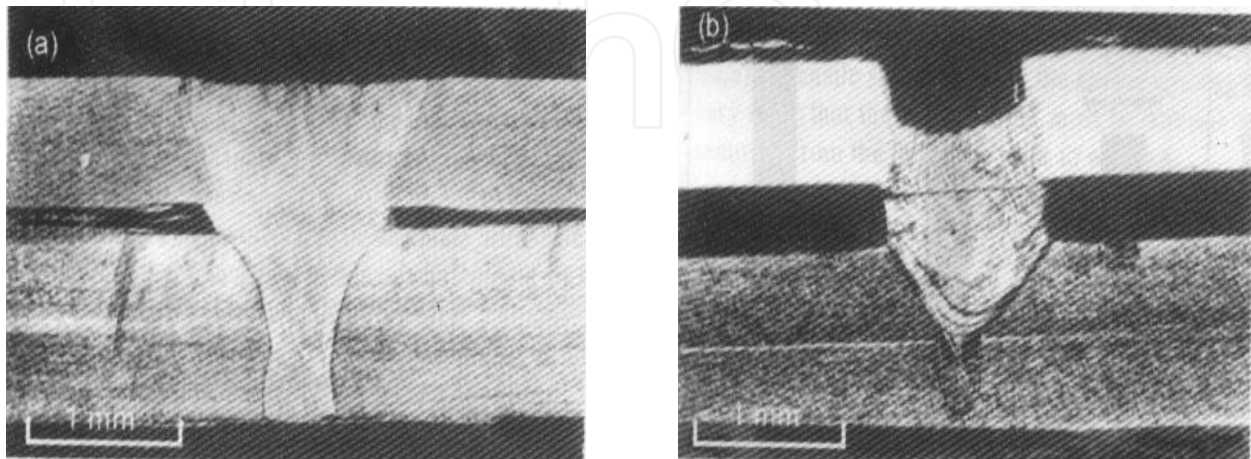

Figure 18. Photographs of cross sections taken from laser lap welds produced using (a) 0.1mm and (b) 0.3mm gap between the sheets.

Generally, there are two mechanisms in laser welding, one is heat conduction under low energy density and the other is deep penetration (keyhole effect) under high energy density. In these experiments, the laser power density when laser beam touched the surface of the top sheet was high enough to melt the metal rapidly and formed the deep penetration. The power density greatly decreased when approached the bottom plate particularly in case of large air gap between both plates that obstructed heat transfer. At this time, the heat transfer was mainly by means of conduction, which could be proved by the weld shape and penetration depth. Based on the weld shape, the fusion lines at both sides of welds were approximately parallel under deep penetration welding conditions, while the fusion line was half circle under heat conduction welding. Consequently, under such experimental conditions, the welding mechanism of lap joints was combination of deep penetration and heat conduction.

Although introducing a small gap between these dissimilar material sheets has resulted in avoiding porosity in weld zone, it has no effect on zinc induced LME cracking in austenitic stainless steel base metal. Figure 19 shows typical example of an optical micrograph of a cross section taken from lap welded joint produced using helium with 15 1/min flow rate and 0.05 mm gap. It is noticed that a sound and uniform weld seam was obtained. However, the most important notice is the formation of LME cracking on grain boundaries of stainless steel base metal as has been explained in the previous section. Cracking were extended for a distance of about 0.5 mm around both sides of lap weld joints. These results of laser welding do conform to other research work concerned with arc welding processes [17].

Generally, the influence of gap between the sheets on weld geometry and quality can be explained using schematic illustrations shown in Figure 20. Since the zinc vapour has no enough access escape route with zero gap, both pores weld with unacceptable profile and LME cracking in stainless steel will be obtained (Figure 20-a). Introducing a small gap between the sheets give the zinc vapour an alternative escape route during welding then, sound and acceptable weld joint will be produced. It should be mentioned that this gap should be limited to an optimum value as has been reported by other researchers [22]. However, the problem is still concerned with LME cracking in austenitic stainless steel base metal around both sides of the joint since it can not be prevented by these measures (Figure 20-b).

2.3.3. Effect of zinc removal prior to welding

The results of the previous two sections confirmed that LME cracking of austenitic stainless steel in laser lap joint with Zn-coated steel is attributed mainly to molten zinc resulted from welding heat. Consequently, this section is concerned with studying this type of cracking as a function of zinc removal prior to welding. In this respect, the effect of both one and two sides grinding of the weld area of Zn-coated sheets was clarified using welding parameters previously resulted in weld zone porosity.
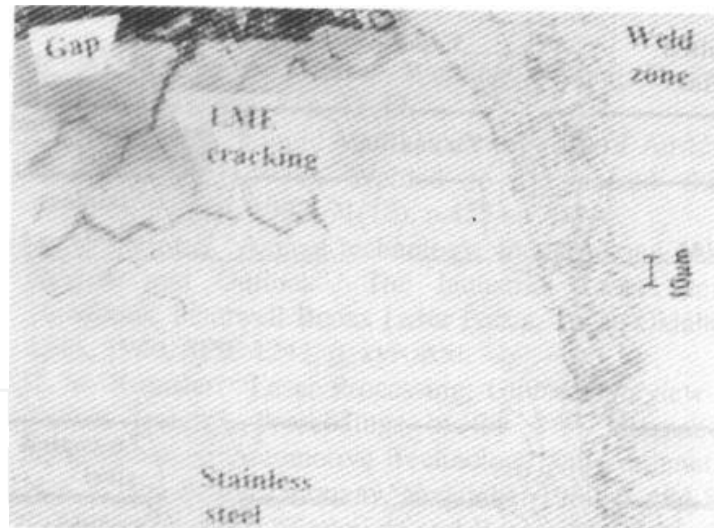

Figure 19. Typical example of optical micrograph of a cross section of lap welded joint produced using 0.05mm gap and 15 l/min helium.

Photographs of laser welds produced without gap between the sheets and with 15 1/min of helium shielding after zinc removal by grinding of weld area from one and two sides are shown in Figure 21-a and b respectively. It can be noticed that removing zinc coating from only one side of Zn-coated sheet was not effective to obtain sound welds since porosity were observed in weld zone (Figure 21-a). In the case of two sides grinding before welding, molten zinc was avoided due to removing of zinc coating then, molten metal was not ejected and this in turn could result in a sound and uniform weld seam (Figure 21-b).
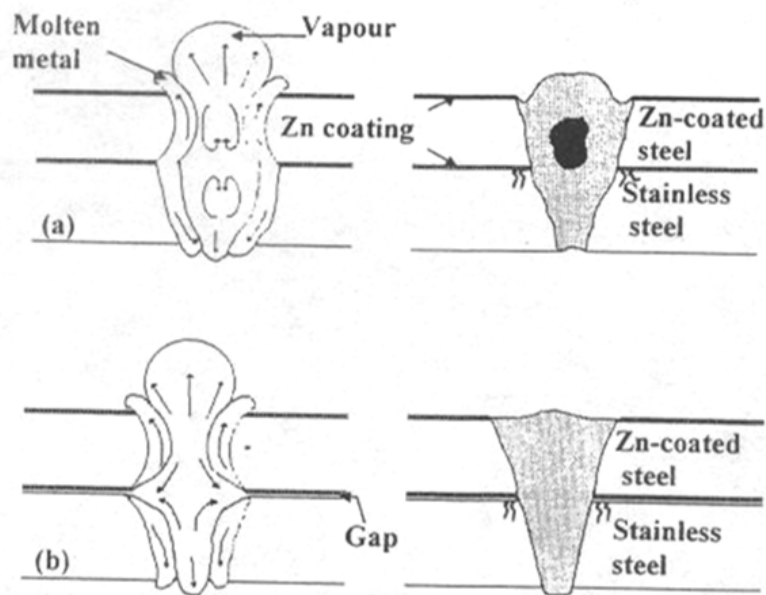
Figure 20. Schematic illustrations showing the effect of introducing a gap between the sheets being welded on weld zone profile, porosity and LME cracking.
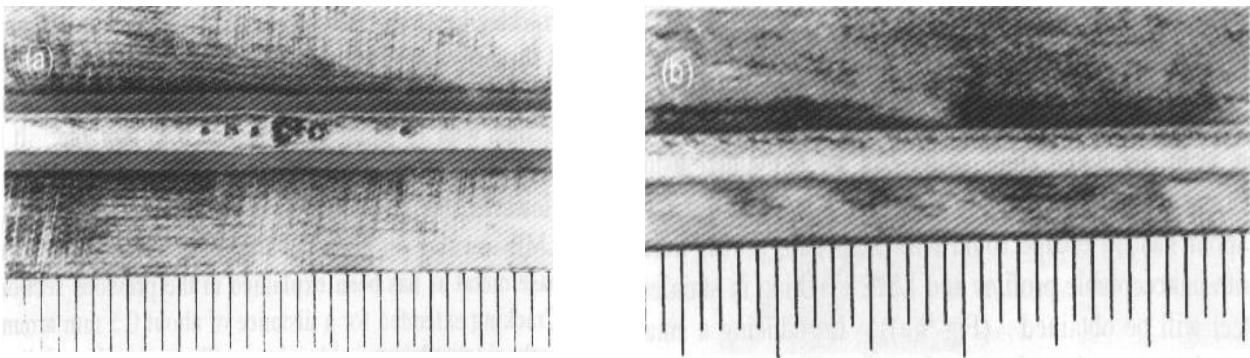

Figure 21. Photographs of laser welds produced using 15 l/min helium shielding and zero gap between the sheets after zinc removal from (a) one side and (b) two sides of the weld area of Zn-coated sheet.
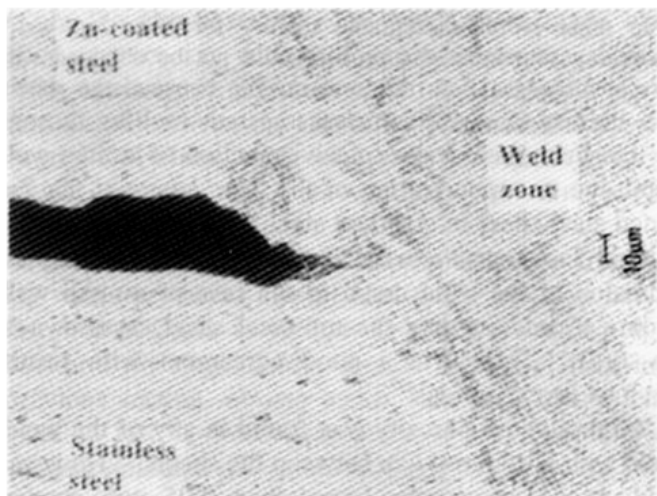

Figure 22. Effect of two sides grinding of weld area of Zinc-coated sheet on LME cracking susceptibility.

In addition, the most important finding in the case of two sides grinding is the disappearance of LME cracking in austenitic stainless steel as shown in Figure 22 that could not be attained in the above two sections. This is due to the complete removal of zinc coatings from the weld area prior to welding.
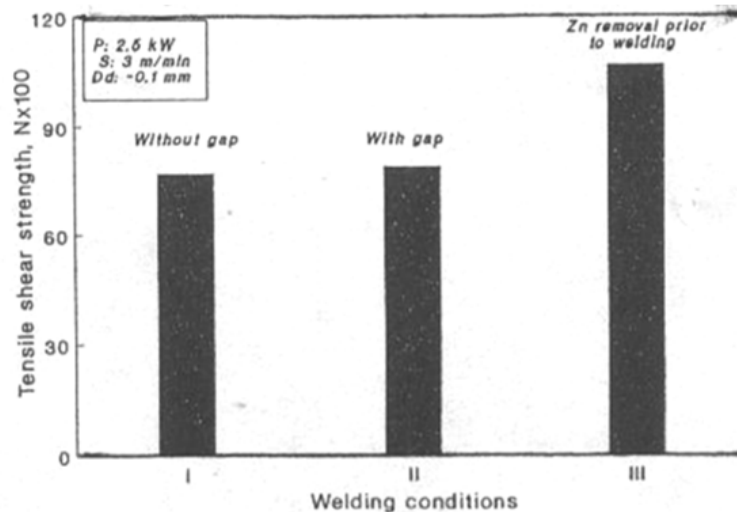

Figure 23. Tensile shear strength of laser lap welded joints as a function of welding conditions used. Welding conditions I, II and III are the optimum conditions used in section 3.3.1, 3.3.2 and 3.3.3, respectively.

Results of tensile shear test of laser lap joints as a function of welding conditions used are shown in Figure 23. Tensile shear strength of joints produced with zinc removal from both sides prior to welding was considerably higher than that of all other joints produced with and without gap regardless of shielding gas type and flow rate. This is attributed to the absence of LME cracking in case of two sides grinding.

Recently, serious industrial incidents of zinc-induced LME cracking in austenitic stainless steel have been reported [29, 30]. The potential for cracking during field welding is certainly greater than the cracking potential in these test specimens. This is due to higher tensile stresses in the case of field welding. Therefore, the removal of galvanized zinc coating prior to welding should be done properly to avoid contamination of austenitic stainless steel with any molten zinc during welding.

3. Conclusion

For CO_2 laser butt welding of similar butt joints of austenitic stainless steels, the following conclusions can be drawn.

- The penetration depth increased with the increase in laser power. However, laser power has a less effect on weld profile.
- Unlike laser power, welding speed has a pronounced effect on size and shape of the fusion zone. Increase in welding speed resulted in an increase in weld depth/width ratio and hence a decrease in the fusion zone size.

- Minimizing heat input and optimizing energy density through optimizing laser power, welding speed, and defocusing distance is of considerable importance for the weld quality in terms of fusion zone size and profile. Helium is more effective than argon as a shielding gas to obtain acceptable weld profile.
- Fusion zone composition was insensitive to change in heat input. However, increase in welding speed and/or decrease in laser power resulted in a finer solidification structure due to low heat input. A dominant austenitic structure with no solidification cracking was obtained for all welds. This could be associated with primary ferrite or mixed mode solidification based on Suutala and Lippold diagrams.
- Mechanical properties, tensile, hardness and bending at room temperature, were not significantly affected by heat input.

For CO_2 laser welding of austenitic stainless steel in lap joints with Zn-coated carbon steel, the following conclusions can be drawn.

- One way to produce sound and uniform laser lap welds of Zn-coated steel with austenitic stainless steel without gap between the sheets is the optimizing shielding conditions. This is of considerable importance for avoiding plasma or preventing porosity and obtaining full penetration without deteriorating the surface quality of the weld. Helium shielding produced noticeably deeper welds while argon exhibited the smoothest top surface. A flow rate of 22 1/min was found to be satisfactory in the case of helium in comparison with 30 1/min for argon.
- The other way to produce sound and homogeneous laser lap welds of these dissimilar materials is the introducing of a small gap (0.025~0.05 mm) between the sheets. Maintaining such gap between the sheets give the zinc vapour an alternative escape route. Smaller gap resulted in pores weld and random instabilities in the weld bead surface while larger gap showed unacceptable levels of drop-through of the weld metal between the sheets.
- To preclude both weld porosity and cracking of the stainless steel by molten zinc in making attachments of Zn-coated steel to 300 series austenitic stainless equipment which in turn will improve tensile shear strength, the choice seems to be very clear that is the zinc coating must be scrupulously removed from the joint area prior to welding.

Recently, new generation of lasers, such as fiber and disk lasers is receiving great attention due to its high efficiency, high power and high beam quality, which can produce an ultra-high peak power density of MW/mm2 levels corresponding to a focused electron beam. These features and advantages of fiber and disc lasers are of considerable importance for deep penetration and high speed welding of austenitic stainless steels with thick sections, which are used in some critical applications such as nuclear power plants. It has been reported that such new generation of lasers is promising to be among the desirable heat sources for deep-penetration high speed welding of thick-section austenitic stainless steels [31-34].

In this regard, multi-passes narrow-gap welding of 50mm thick 316L plates has been investigated using 8 kW disk laser where the effect of welding conditions on the weld bead

geometry and welding defects was studied. It is reported that butt joint of 50 mm thick plates with narrow gap could be performed with eight-layers welding at laser power of 6 kW and welding speed of 0.4 m/min. In order to reduce the weld passes further, gas jet assisted laser welding was tried to weld thick 316L plates with a 10 kW fiber laser. The result showed that butt-joint welding of 40 mm plates without filler wire could be carried out at 0.3 m/min welding speed with no porosity or other welding defects. As for 50 mm thick plate, a good weld bead could be obtained with bead-on-plate welding from both sides at 0.2 m/min welding speed [35].

Author details

Abdel-Monem El-Batahgy
Manufacturing Technology Department, Central Metallurgical R & D Institute, Cairo, Egypt

Acknowledgement

4. References

[1] Zacharia, T.; David, S. A.; Vitek, J. M. & Debroy, T. (1989). *Metall. Trans.* 20 A, 1125.

[2] Suutala, N. (1983). *Metall. Trans.* 14 A, 191.

[3] Klimpel, A. & Lisiecki, A. (2007). Laser Welding of Butt Joints of Austenitic Stainless Steel AISI 321. *Journal of Achievements in Materials and Manufacturing Engineering*, 25, 1.

[4] Curcio, F.; et al. (2006). Welding of Different Materials by Diode Laser. *Journal of Materials Processing and Technology,* 175, 83-89.

[5] Zacharia, T.; David, S. A.; Vitek, J. M. & Debroy, T. (1989). *Welding Journal*, 68, 12.

[6] David, S. A.; Vitek, J. M. & Hebble, T. L. (1987). *Welding Journal.* 66, 289.

[7] Schaeffler, A. L. (1949). *Metal Progr.* 56, 680.

[8] Kujanpaa, V.; Suutala, N.; Takalo, T. & Moisio, T. (1979). *Welding Research Int.* 9, 55.

[9] Vitek, J. M. & David, S.A. (1982). *ASM Conference Proceedings*, Trends in Welding Research in the United States (ASM, Metals Park, Ohio,) pp.243-258.

[10] Lippold, J. C. (1985). *Welding Journal*, 64, 127.

[11] Kotecki, D. & Siewert, T. A. (1992). *Welding Journal* 71, 171.

[12] Lippold, J. C. (1994), *Welding Journal.* 73, 129.

[13] Dilthey, U. & Risch, A. (2001). Laser Welding of Stainless Steels and Stainless Low-Alloy Material Combinations, *Welding in the World*, 36, 67-71.

[14] Elmer, J. W.; Alien, S. M. & Eagar, T. W. (1990). *Recent Trends in Science and Technology*, eds. David S. A. & Vitek J. M. (ASM International, Materials Park, Ohio, pp. 165-170.

[15] Brooks, J. A. & Thompson, A. W. (1991). *Inst. Met. Reviews*, 36, 16.

[16] Metzbower, E. A. (1991). Laser Welding, *Naval Engineers Journal*, Vol. 8, p. 41-49

[17] Bruscato, R. M. (1992). Liquid Metal Embrittlement of Austenitic Stainless Steel When Welded to Galvanized Steel. *Welding Journal*, 71(12), p.455s-459s.

[18] Belforte, D. A. (1990). Annual technology, Industry, and Market Review and Outlook. *The Industrial Laser Annual Handbook*, Pennwell Books Laser Focus, Tulsa, Oklahoma USA, SPIE 1241, p. xvi-xxxi.

[19] Roessler, D. M. (1989). Laser Processing-Global Overview and Future Trends. *Proceedings of the 21st International Symposium on Automotive Technology and Automation*, Vol. 1, Wiesbaden, Germany, November 1989, p. 494-516.

[20] Marinono, G.; et al. (1989). Technical and Economic Comparison of Laser Technology with The Conventional Technologies For Welding. *Proceedings of the 6th Int. Conf. on Laser in Manufacturing*, IFS, May 1989, ISBN 1-85423-047-6, p.105.

[21] Beyer, E. & Gasser, E. (1987). Plasma Fluctuations in Laser Welding With CW CO2-Lasers. *Proc. of The 6th Int. Cong. on Appl. Lasers and Electro-Optics, ICALEO '87*, San Diego, California, November 1987, p. 17-23.

[22] Bagger, C.; Miyamoto, I.; Olsen, F. & Maruo, H. (1992). Process Behaviour During High Power CO2 Laser Welding of Zinc Coated Steel. *Proceedings of LAMP*, Nagaoka, Japan, June 1992.

[23] Akhter, R.; Steen, W. M. & Cruciani, D. (1988). Laser Welding of Zinc Coated Steel. *Proc. of The 5th Int, Cong. on Lasers in Manufacturing, LIM 5*, Stuttgart, West Germany, September 1988, p. 195-206.

[24] Heyden, J.; Nilsson, K. & Magnusson, C. (1989). Laser Welding of Zinc Coated Steel, *Proc. of The 6th Int, Conf. on Lasers in Manufacturing, LIM 6*, May 1989, p. 93-104.

[25] Graham, M. P.; Hirak, D. M.; Kerr, H. W. & Weckman, D. C. (1994). Nd-YAG Laser Welding of Coated Sheet Steel. *Journal of Laser Applications*, Vol. 6, p. 212-222.

[26] Stoloff, N. S. (1977). Recent Development in Liquid Metal Embrittlement. *Proceedings Conference on Environment Sensitive Mechanical Behavior*, AIME, Chicago, 1977.

[27] Nicholas, M. G. & Old, C. F. (1979). Review of Liquid Metal Embrittlement. *Journal of Material Science*, Vol. 14, p. 1-18.

[28] Tzeng, Y. (2006). Gap-free lap welding of zinc-coated steel using pulsed CO2 laser. *International Journal of Advanced Manufacturing and Technology*, 29, 287-295.

[29] Johnson, J. M.; Berry, M. R. & Gutzeit, J. (1982). Zinc Embrittlement of Stainless Steel welds. *Proceedings of AIME Meeting on Embrittlement by Liquid and Solid Metals*, St. Louis, MO, 1982.

[30] Shinohara, T. & Matsumoto, K. (1982). Welding Cracks of Zn-contaminated Stainless Steel Pipe. *Corrosion Science*, 22(8), p.723-737.

[31] Thomy, C.; Seefeld, T. & Vollertsen, F. (2005). Proceedings of the Third International WLT-Conference on Lasers in Manufacturing, Munich, Germany, pp.27-32.

[32] Verhaeghe, G. & Hilton, P. (2005). Proceedings of ICALEO, Miami, USA, pp.264-271.

[33] Liu, S.; Kutsuna, M. & Xu, G. (2006). Proceedings of ICALEO, Scottsdale, USA, pp.562-568.

[34] Reem, S. (2006). Proceedings of ICALEO, Scottsdale, USA, pp.586-594.

[35] Zhang, X.; Ashida, E.; Tarasawa, S.; Anma, Y.; Okada, M.; Katayama, S. & Mizutani, M. (2011). Welding of thick stainless steel plates up to 50 mm with high brightness lasers. Journal of Laser Applications, **23**, 022002 (2011); http://dx.doi.org/10.2351/1.3567961